Nonisothermal, Uncontrolled Homo- and Copolymerization of Ethylene Using Selected Zirconocenes

MUHAMMAD ATIQULLAH, HASSAN HAMMAWA, MUHAMMAD N. AKHTAR, JAVAID H. KHAN, HALIM HAMID

Center for Refining and Petrochemicals, The Research Institute, King Fahd University of Petroleum & Minerals, Dhahran 31261, Saudi Arabia

Received 27 August 1997; accepted 25 January 1998

ABSTRACT: Nonisothermal, uncontrolled polymerization, conducted in varying mixing regimes, offered a facile methodology to evaluate the influence of several important process development factors such as mixing, reaction exotherm, and thermal perturbations on the catalytic activity and kinetic stability, polymerization performance, and properties of the resulting polymers. Ethylene was homo- and copolymerized with hexene-1 under varying impeller speeds (hence, thermal perturbations), using Ind_2ZrCl_2 and $Et(Ind)_2ZrCl_2$ and the MAO cocatalyst. With respect to the effects of the above process development factors, the following was observed: The reaction exotherm profiles, tracing the polymerization history, qualitatively represented the kinetic profile and the catalytic stability. The unbridged Ind_2ZrCl_2 was shown to be more stable than the bridged $Et(Ind)_2ZrCl_2$. With change in the level of stirring from a diffusion-controlled regime to a nondiffusion-controlled, external gas–liquid mass-transfer resistance-free one, the reaction exotherm and the run time-average catalytic activity increased. So far as the influence of the chiral versus the achiral zirconocene structure is concerned, the copolymer composition distribution and soluble fraction generated by chiral $Et(Ind)_2ZrCl_2$ were more sensitive to the mixing conditions and thermal perturbations than were those produced by achiral Ind_2ZrCl_2. $Et(Ind)_2ZrCl_2$ produced higher molecular weight backbones, incorporated more hexene-1 and chain branching, and introduced less crystallinity in the copolymers than did Ind_2ZrCl_2. The influence of Ind_2ZrCl_2 on higher-weight homopolymer backbones was opposite to that of $Et(Ind)_2ZrCl_2$. Incorporation of hexene-1 significantly decreased the average molecular weights and density and increased the run-time-dependent average catalyst activity. A positive comonomer effect took place. The bulk polymer properties did not critically depend on the mixing state. Thermal perturbations broadened the polydispersity index. © 1998 John Wiley & Sons, Inc. J Appl Polym Sci 70: 137–147, 1998

Key words: zirconocene catalyst; nonisothermal olefin polymerization; CRYSTAF; comonomer and molecular weight distributions; chain branching; DSC

INTRODUCTION

It has been predicted that metallocene catalysts will forge the future of ethylene polymerization technology beyond the year 2000. In order that this prediction comes true, research orientation has been toward developing competent polymerization processes. A key factor that influences this aspect is the role that temperature plays on the polymerization reaction. Therefore, we review as follows the effect of temperature with the variation of metallocene structures on the catalytic activity in presence of the methylalumoxane (MAO) cocatalyst and on the properties of the resulting polyethylenes.

Correspondence to: M. Atiqullah. (matiq@kfupm.edu.sa)

Contract grant sponsor: Research Institute of the King Fahd University of Petroleum & Minerals at Dhahran, Saudi Arabia.

Journal of Applied Polymer Science, Vol. 70, 137–147 (1998)

 CCC 0021-8995/98/010137-11

For Ind_2ZrMe_2 and Cp_2ZrPh_2, the polyethylene productivity was maximum at about 50°C. However, Ind_2ZrMe_2 was, overall, more active.[1] On the other hand, for Cp_2ZrCl_2, an optimum temperature range of 50–80°C was found.[2,3] This shows that the Cl ligand, unlike the Ph ligand, broadened the optimum polymerization temperature. (*neo*-MeCp)$_2ZrCl_2$ showed a monotonic increase in ethylene polymerization activity without showing any maximum between 10 and 90°C, which may be attributed to the increased coordinated anionic propagation rate due to electron donation. Also, the induction period shortened with the increase in the polymerization temperature.[4]

With Et(Ind)$_2ZrCl_2$, increasing the temperature from −20 to 70°C increased the maximum ethylene polymerization rate by a factor of 5000.[5] For the copolymerization of ethylene with butene-1 at 30 and 50°C, the rate of ethylene consumption reached a maximum as the butene-1 concentration in the reaction mixture increased. At 70°C, the maximum reaction rate decreased with increase in the butene-1 concentration.

Increasing the polymerization temperature decreased the molecular weight and polydispersity index of the resulting polyolefins, irrespective of the variation of the σ-ligand and transition-metal type.[2–6] A similar effect of temperature on the melting point of polyethylenes, which occurred probably because of the presence of oligomers or structural defects, was evidenced.[2,4]

The above work on isothermal, metallocene-catalyzed ethylene polymerization has several limitations from the process development viewpoint which we summarize as follows: It does not illustrate the influence of a number of important process development factors such as mixing, reaction exotherm, kinetic stability of the experimental metallocenes, and thermal perturbations on the catalytic activity, polymerization performance, and the properties of the resulting polymers. The significance of the effects of mixing on the polymerization reactions and on the properties of the resulting polymers has already been reported to be a key issue in the literature.[7–11] The critical polymer properties include the microstructural ones, that is, the molecular weight and copolymer composition distributions. These property distributions influence the density, melt-flow index, melt strength of the resin, as well as melt blending with the processing additives and selection of processing/fabrication methods.[12] All these eventually affect the performance of the end products which is reflected by the resistance to stress cracking, impact, creep, additive migration, etc.[12,13]

Also, the polymerization temperature varies during start-up and under thermal runaway and inadvertent situations causing failure of a temperature controller. The resulting polymerization environment related to the reaction mass differs from that when the same polymerization will be conducted isothermally even by varying the polymerization temperature from one run to another.

Based on the above discussion, we concluded that a facile experimental methodology should be developed that can evaluate the influence of the above process development factors, which is currently unavailable in the literature. Discrete isothermal polymerization runs cannot be applied because they, on principle, suppress the growth of the reaction exotherm and thermal perturbation. Additionally, they are time-consuming and cumbersome. On the other hand, the uncontrolled, nonisothermal polymerization mode holds promise in this respect, while we know that under a set of given experimental conditions the rate of generation of the catalytically active metallocenium ion is related to the measured reaction exotherm profile. Moreover, the nonisothermal polymerization approximates a limiting case of thermal perturbations. Therefore, we undertook the current study, the objectives of which were as follows:

(i) Evaluate the potential application of the nonisothermal, uncontrolled polymerization mode to measure the influence of the above process development factors by conducting homopolymerization of ethylene and its copolymerization with hexene-1 using Ind_2ZrCl_2 and Et(Ind)$_2ZrCl_2$ in the presence of MAO in a semibatch, laboratory-scale reactor under varying mixing conditions;
(ii) Characterize the properties of the resulting polyolefins in terms of thermal characteristics, molecular weight distribution and its averages, and composition distribution and its averages; and
(iii) Determine the influence of the metallocene structures (bridged versus unbridged configurations), thermal perturbations, and polymerization conditions (reaction exotherm profile and level of mixing) on the above polyolefins properties.

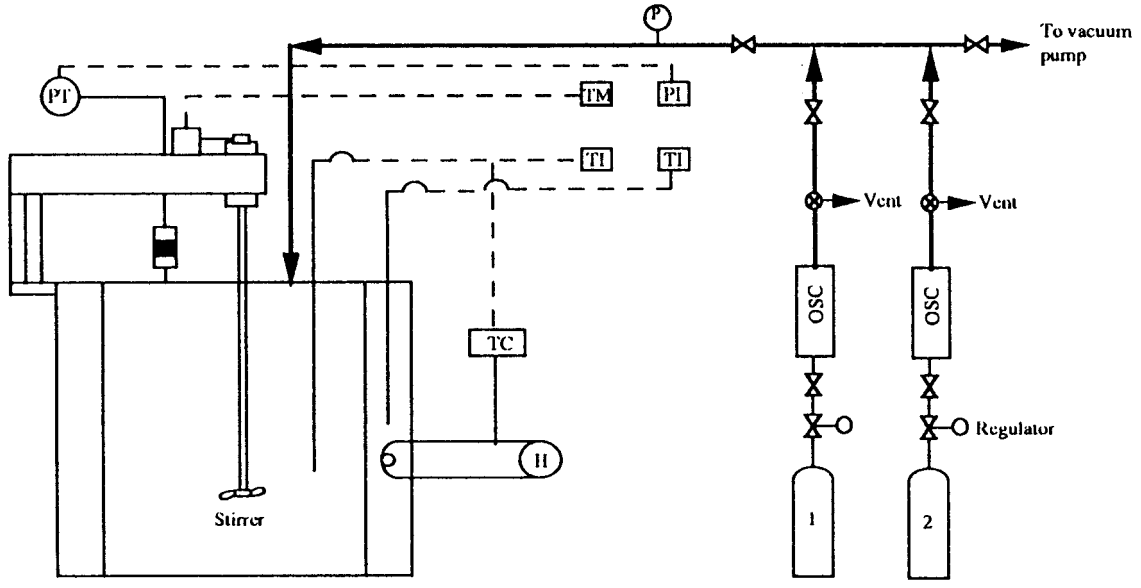

1	Ethylene	2	Argon
H	Heater	P	Pressure Gauge
TI	Temperature indicator	PT	Pressure Transducer
TC	Temperature Controller	TM	Tachometer
OSC	Oxygen Scavenging Column	PI	Pressure indicator
⋈	Valve		

Figure 1 Schematic of the experimental polymerization setup.

EXPERIMENTAL

Chemicals

$(Ind)_2ZrCl_2$, $Et(Ind)_2ZrCl_2$, and MAO (10% by weight in toluene with an average molecular weight of 800 and degree of oligomerization of 14) were procured from Witco (Bergkamen, Germany). Toluene was purchased from BDH (Poole, England, UK) and dried by refluxing in a Na/benzophenone mixture for approximately 2 days until a dark blue color was obtained. All manipulations were carried out in an inert atmosphere of argon. Ethylene, 99.95% pure, and argon, 99.999% pure, were obtained from the Saudi Industrial Gas Co. (Dammam, Saudi Arabia). Hexene-1 was donated by Chevron (Geneva, Switzerland).

Polymerization

Figure 1 shows the reactor setup that was used to conduct the polymerization runs. 1 L Parr reactor, equipped with a pitched-blade turbine impeller with a speed controller, external heating jacket, thermowell, and pressure transducer, was used. A panel digitally displayed the impeller speed, outer jacket temperature, and internal reactor temperature and pressure. Table I summarizes the overall polymerization conditions in the footnote.

A typical ethylene homopolymerization run was carried out as follows: First, the experimental zirconocene catalyst was separately preactivated under argon with the MAO cocatalyst to generate the active zirconocenium cation. Note that preactivation of the metallocene with MAO has been reported to enhance the catalytic activity.[14–19] For this purpose, a few milligrams (about 3–6 mg) of the zirconocene was dissolved in about 5 mL of dry toluene. The required amount of the resulting solution was mixed at 50°C with a calculated amount of the MAO solution for at least 20 min.

Next, toluene was introduced into the reactor. The reactor was then successively pressurized with argon to about 30 psia and evacuated three times. Following this, the previously fed toluene solvent was heated to the desired starting tem-

Table I Polymerization Activity of the Experimental Zirconocenes and the Thermal Characteristics of the Resulting Polymers

Polymerization Run No.	Catalyst Type	Level of Stirring (rpm)	Peak Reaction Exotherm (°C)	Catalyst Activity (kg PE/[mol Zr h])	Peak Melting Point (°C)	Density (g/cm^3)	T_w (°C)	T_n (°C)	$T_w : T_n$
Ethylene homopolymerization									
H1	Ind_2ZrCl_2	950	35	4386.5	135.8	0.949	85.3	86.3	0.989
H2	$Et(Ind)_2ZrCl_2$	950	41	4201.6	134.4	0.962	81.7	82.2	0.994
Ethylene copolymerization with hexene-1									
C1	Ind_2ZrCl_2	450	40	5586.6	124.3	0.938	63.4	59.8	1.061
C2	Ind_2ZrCl_2	950	50	7492.9	123.0	0.936	62.4	58.4	1.069
C3	$Et(Ind)_2ZrCl_2$	450	40	7044.7	129.8	0.918	68.0	61.1	1.113
C4	$Et(Ind)_2ZrCl_2$	950	56	7128.9	126.1	0.922	59.2	53.8	1.101

Ethylene feed pressure: 31 ± 1 psi; temperature: 50 ± 1°C; catalyst concentration: ~ 23.5 μmol Zr/L solvent; initial hexene-1 concentration: ~ 240.0 mmol/L; cocatalyst-to-catalyst ratio (AL : Zr molar ratio): ~ 2,383. T_w and T_n are weight-average and number-average solution crystallization temperatures, respectively.

perature (~ 50°C), then saturated with ethylene. After that, the preactivated zirconocene was injected into the reactor through a septum such that the desired catalyst concentration and Al : Zr ratio (see Table I) were achieved in about 250 mL of the reaction mixture. Ethylene was fed into the reactor for 1 h in a semi-batch mode. This semi-batch operation replenished the consumed amount, thereby maintaining a constant polymerization pressure (see Table I). The polymerization temperature was monitored as a function of the reaction time.

Ethylene and argon were passed through a Hewlett–Packard oxygen trap before feeding the reactor. The reactor content was continuously stirred following the addition of toluene.

The polymerization was quenched by stopping the ethylene supply, venting the reactor, and adding 5–7 mL of methanol acidified with 2.5 vol % HCl. About 75 mL of the acidified methanol was further added for complete precipitation of the polymer. At this stage, the impeller speed was reduced to ~ 300 rpm and the resulting polymer suspension reached room temperature. Subsequently, it was filtered using a fritted glass filter funnel and washed several times with the acidified methanol. The filtered polymer was then dried 10–12 h under a vacuum to a constant weight.

Ethylene was copolymerized with hexene-1 following the above homopolymerization procedure. However, in this case, toluene was mixed with the desired quantity of hexene-1, then was added to the reactor under argon.

The polymerization runs were conducted at 450 and 900 rpm, which correspond to two distinct mixing regimes: diffusion-controlled and nondiffusion-controlled and gas–liquid mass-transfer resistance-free, respectively.[10,20,21]

Polyolefin Characterization

Thermal Properties

DSC Analysis. The synthesized polyethylene samples (see Table I) were thermally characterized using a Perkin–Elmer differential scanning calorimeter (Model DSC-4) attached to a System-4 microcomputer controller. First, the calorimeter was calibrated using indium which melts at 156.6°C with a heat of fusion of 6.8 cal/g. The sample compartment was purged with argon during operation. About 5.0 mg of the experimental polymer was sealed in an aluminum sample pan using a Universal crimper press. The pressed

sample was heated at 20°C/min to 170°C. Note that such a heating rate was used to prevent recrystallization of the polyolefin backbone chains while they melted during heating. The data were stored and analyzed using the Model 3600 data station. The baseline was established by tangentially joining the ending (postmelting) isothermal line with the starting (premelting) one. The intersections of this tangent with the thermogram determined the lower and upper temperature limits of integration. The integrated area under this curve gave the heat of fusion. The percentage crystallinity was obtained by dividing this heat of fusion with 68.4 cal/g,[22] the heat of fusion of a 100% crystalline polyethylene.

Crystallization Fractionation (CRYSTAF) Analysis. The copolymer composition distribution was qualitatively measured using the recently developed crystallization analysis fractionation (CRYSTAF) equipment. CRYSTAF monitors the polymer solution concentration as the polymer molecules having the same number of side-chain branching crystallize/precipitate at the same temperature during cooling. Aliquots of the solution are filtered and analyzed by a differential refractometer concentration detector. Further details and a description of the CRYSTAF equipment are available elsewhere.[23] Standard operating conditions were employed for the CRYSTAF analysis. The weight- and number-average solution crystallization temperatures of the copolymers T_w and T_n, respectively, were calculated using the following expressions[24]:

$$T_w = (\sum c_i T_i)/\sum c_i \quad (1)$$

$$T_n = \sum c_i/(\sum c_i/T_i) \quad (2)$$

where c_i and T_i are the concentration and crystallization temperature, respectively, of the postprecipitated polymer-solution fraction i.

Preparation of Polymer Film Samples

The film samples, 130 micron thick, were prepared using a laboratory Carver press (Model C). The temperature of the heating plates was set between 145 and 150°C to ensure complete melting of the samples. About 300–400 mg of the polymer was placed on the press plate. When the polymer melted, it was pressed from the top with a load of 10 tons for about 5 min. Following this, the press was cooled to about 90°C by circulating a mixture of water and air and was left under the same load for 1 h. The temperature was brought to that of the ambient by circulating water. The above operation produced a homogeneous, transparent polymer film.

Average Copolymer Composition Determination

The average composition of the synthesized copolymers was determined using FTIR spectroscopy in terms of chain branching (methyl groups/1000 C) and the average hexene-1 composition following the ASTM standard D 2238-86 procedure.[25] The FTIR spectra of the previously prepared films were recorded by a Perkin–Elmer spectrometer (Model 1650) which was calibrated using a standard polystyrene film. The sample compartment was continuously purged with nitrogen. A typical spectrum was obtained using 40 scans and a spectral resolution of 1 cm^{-1}. After Fourier transformation of the interferograms, a difference spectrum was obtained by subtracting the spectrum of an HDPE (density = 0.964 g/cm^3) film from that of the experimental copolymer film (see Fig. 2). The resulting difference spectrum had a peak position reproducibility of 0.1 cm^{-1}. The butyl branches were identified from the methyl symmetrical deformation band around 1378 cm^{-1} and were calculated using the following expression[25]:

$$\frac{\text{Methyl groups}}{1000\text{C}} = f_{1378} \times \frac{A_{1378}}{dt} \times 10 \quad (3)$$

where $f_{1378} = 0.110$ is a conversion factor. A_{1378} is the corrected absorbance at 1378 cm^{-1}, and d and

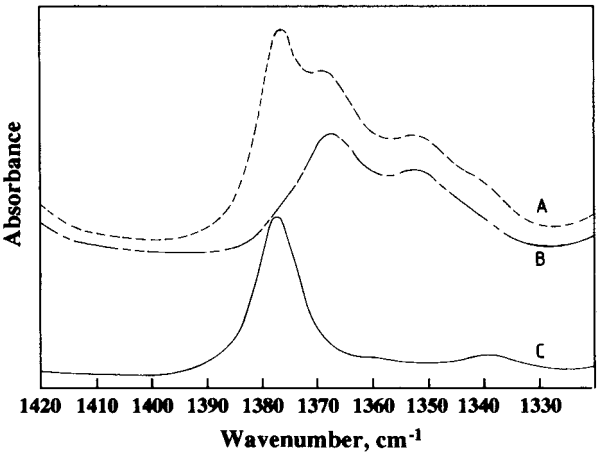

Figure 2 FTIR spectra: (A) an experimental ethylene/hexene-1 copolymer; (B) a commercial polyethylene (density ~ 0.964); (C) difference spectrum.

t are the density and thickness, respectively, of the polymer film. The film thickness was measured using a micrometer and the density was determined as follows:

Measurement of Density

The synthesized polymers were extruded through the die of a melt flow indexer. The extrudate was cut into small pieces which were mildly melted and pressed using a laboratory Carver press to expel the entrapped air. The density of this air-free polymer sample was measured according to the procedure detailed about the calibration of standard glass floats in ASTM D 1505-85.[26]

The polymer sample was dipped into a uniform mixture of water and i-propanol contained in a measuring cylinder at 24°C. The water : i-propanol ratio was varied until the sample attained an equilibrium height. Under this situation, the density of the mixture equaled that of the sample. The mixture density was measured by injecting about 2.0 mL of the mixture into an automatic liquid density meter (DMA 48).

Gel Permeation Chromatographic Analysis

The molecular weight distributions and the average molecular weights of the synthesized polymers were measured using a Polymer Laboratories GPC 210 equipment. The samples were dissolved at 150–160°C in 1,2,4-trichlorobenzene (TCB) containing 0.05% 2,6-di-*tert*-butyl-4-methyl phenol (BHT) antioxidant. The resulting solution was periodically shaken without applying any high shear stirring. Aliquots of the hot polymer solutions were transferred in vials to the autosampler where the warm zone was maintained at 80°C, and the hot zone, at 160°C.

The equipment was calibrated using polystyrene standards (EasiCal PS-1). The polystyrene-based calibration curve was next converted into the universal one using the Mark–Houwink constants of polystyrene and polyethylene.[27] Standard operating conditions were used for the GPC analysis.

RESULTS AND DISCUSSION

Table I summarizes the catalytic activity and the thermal characteristics of the synthesized polymers as a function of the level of stirring and the zirconocene structural variation. The level of stirring corresponding to 450 and 950 rpm refers to diffusion-controlled and nondiffusion-controlled, external gas–liquid mass-transfer resistance-free regimes of mixing, respectively. With respect to the nondiffusion-controlled regime of mixing, the run time-average copolymerization catalytic activity and the peak reaction exotherm increased, irrespective of the variation in zirconocene structures. At 950 rpm, the copolymerization catalytic activity and the peak reaction exotherm exceeded those in homopolymerization where Ind_2ZrCl_2 showed a little higher activity than that of $Et(Ind)_2ZrCl_2$. The converse was the influence of the zirconocene structural variation on the reaction exotherm.

At 450 rpm, $Et(Ind)_2ZrCl_2$ showed higher copolymerization activity than did Ind_2ZrCl_2. This finding matches what Chien and He[28] observed with the isothermal copolymerization of ethylene and propylene catalyzed by $Et(H_4Ind)_2ZrCl_2$ and Ind_2ZrCl_2. Note that the common characteristics of the comonomers hexene-1 and propylene are structurally prochiral.

Figure 3 shows that all the polymerization runs proceeded without an induction period. Each reaction exotherm profile was of a decay type having the following characteristics:

(i) Buildup or acceleration period during which the polymerization rate increased until it reached a maximum;
(ii) Decay period during which the polymerization rate decreased after reaching the maximum value; and
(iii) The catalytically active zirconocenium cation was generated during the buildup or acceleration period, whereas during the decay period, the opposite happened, reducing the activity.

Given the same impeller speed, the reaction exotherm profiles of the copolymerization runs were above those of the corresponding homopolymerization ones. This evidences that a positive comonomer effect occurred during the reaction period. The run-time-dependent average catalyst activities also support this finding (see Table I). Various reasons that have been proposed to explain this comonomer effect are available elsewhere.[29,30]

The reaction exotherm profiles also demonstrate the catalytic systems' stability which may be qualitatively approximated by the difference between the maximum and the terminal reaction

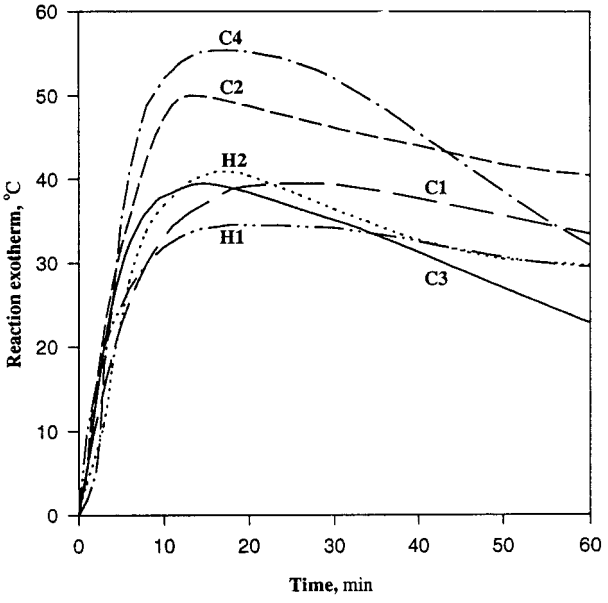

Figure 3 Effect of zirconocene structures and impeller speed on reaction exotherm profiles. H1: 950 rpm, Ind_2ZrCl_2; H2: 950 rpm, $Et(Ind)_2ZrCl_2$; C1: 450 rpm, Ind_2ZrCl_2; C2: 950 rpm, Ind_2ZrCl_2; C3: 450 rpm, $Et(Ind)_2ZrCl_2$; and C4: 950 rpm, $Et(Ind)_2ZrCl_2$.

exotherm values. The greater is the difference, the less stable is the catalyst. Based on this criterion, the unbridged Ind_2ZrCl_2 turned out to be stabler than the bridged $Et(Ind)_2ZrCl_2$, independent of the polymerization type and the impeller speed. Note that the reaction exotherm profiles represent a qualitative equivalence of the polymerization kinetic profiles which also show the catalytic stability. Additionally, the reaction exotherm profiles traced the polymerization history and the associated thermal perturbations. The following text summarizes the thermal properties of the synthesized polymers.

The weight- and number-average solution crystallization temperatures (T_w and T_n) of the copolymers, like the corresponding polymer peak melting temperatures, were below those of the ethylene homopolymers which are essentially linear. Therefore, the side-chain branching, resulting from the incorporation of hexene-1, affected the solid-state melting and solution crystallization in a similar fashion. The effect of side-chain branching on the ratio of $T : T_n$ revealed the following: For the homopolymers, $T_w : T_n < 1$, whereas for the copolymers, $T_w : T_n > 1$. The peak melting temperature and the density of the copolymers were lower than those of the homopolymers.

Table II shows that incorporation of hexene-1

Table II Microstructural Characteristics of the Synthesized Ethylene Homo- and Copolymers

Polymerization Run No.	Catalyst Type	Chain Branching (CH_3 group/1000 C)	Crystallinity (%)	Average Hexene-1 Composition (mol %)	Weight-average Molecular Weight (g/mol)	Number-average Molecular Weight (g/mol)	PDI[a]	Soluble Fraction
Ethylene homopolymerization								
H1	Ind_2ZrCl_2	Not applicable	81.52	Not applicable	196,184	81,358	2.4	0.0
H2	$Et(Ind)_2ZrCl_2$	Not applicable	80.29	Not applicable	116,994	17,937	6.5	0.0
Ethylene copolymerization with hexene-1								
C1	Ind_2ZrCl_2	18	57.07	3.9	27,130	4,619	5.8	3.3
C2	Ind_2ZrCl_2	18	57.98	3.9	23,921	5,257	4.6	6.0
C3	$Et(Ind)_2ZrCl_2$	20	36.14	4.3	43,954	11,579	3.8	13.7
C4	$Et(Ind)_2ZrCl_2$	22	36.66	4.8	46,770	9,688	4.8	6.6

[a] PDI, polydispersity index.

affected the microstructure of the synthesized polymers in terms of change in (a) molecular weight (polymer backbone length), (b) side-chain branching (crystallinity), and (c) soluble fraction. What follows categorically describes these microstructural changes as well as the resulting composition distributions.

The weight- and number-average molecular weights of the copolymers dramatically decreased, irrespective of the variation of the zirconocene structures and the impeller speed. Here, $Et(Ind)_2ZrCl_2$ produced higher molecular weight polymers than did Ind_2ZrCl_2. However, with the homopolymers, the unbridged versus bridged (achirality versus chirality) structural effect of the zirconocenes on the molecular weight was the opposite; Ind_2ZrCl_2 synthesized higher molecular weight polymers than did $Et(Ind)_2ZrCl_2$. These results conform to what Lehtinen and Löfgren[31] found with the isothermal (a) homopolymerization of ethylene using the same zirconocenes and (b) copolymerization of ethylene with propylene by Cp_2ZrCl_2 and $Et(Ind)_2ZrCl_2$.

The molecular weight was found to be inversely related to the corresponding run time-dependent average catalyst activity (see Tables I and II). Note that metallocene-catalyzed isothermal polymerization also shows the same inverse relation between molecular weight and activity.[32]

In the above polymerization runs, the chain-transfer rate increased over the propagation rate which decreased the molecular weight.[33] The causes of the increased chain transfer rate may be summarized as follows.

(i) In homopolymerization, the C_2 symmetric chirality of $Et(Ind)_2ZrCl_2$ enhanced the termination rate due to the β-H elimination rate over that of Ind_2ZrCl_2.

(ii) In copolymerization, apart from β-H elimination, hexene-1 acted as a chain-transfer agent[34] or (b) an additional chain-transfer mechanism competed with the β-H elimination.[28] A possible mechanism is the σ-bond metathesis reaction of the propagating species with ethylene, which is shown below:

$$Zr—CH_2—CH_2—P + C_2H_4 \rightarrow Zr—CH{=}CH_2 + PC_2H_5 \quad (4)$$

(P = growing copolymer chain)

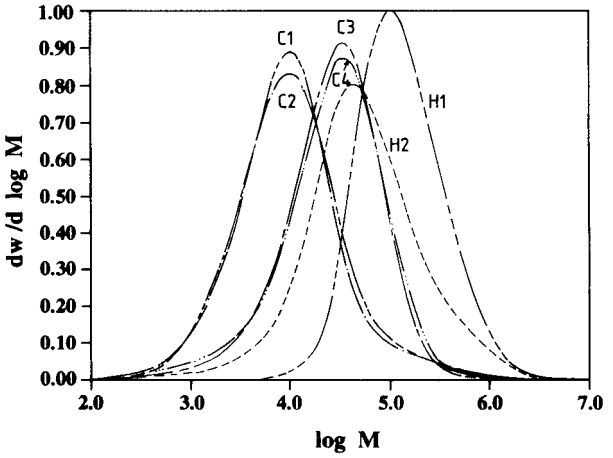

Figure 4 Effect of zirconocene structures and impeller speed on molecular weight distributions profiles. H1: 950 rpm, Ind_2ZrCl_2; H2: 950 rpm, $Et(Ind)_2ZrCl_2$; C1: 450 rpm, Ind_2ZrCl_2; C2: 950 rpm, Ind_2ZrCl_2; C3: 450 rpm, $Et(Ind)_2ZrCl_2$; and C4: 950 rpm, $Et(Ind)_2ZrCl_2$.

$$Zr—CH{=}CH_2 + n\,C_2H_4 \rightarrow Zr—(CH_2)_{2n}—CH{=}CH_2 \quad (5)$$

(iii) In copolymerization, the C_2 symmetric chirality of $Et(Ind)_2ZrCl_2$ so affected the β-H elimination, chain transfer by hexene-1, and the σ-bond metathesis reaction that the resultant termination rate was lower than that of Ind_2ZrCl_2.

The polydispersity indices listed in Table II illustrate that the nonisothermal operation produced broader molecular weight polymers than what an isothermal operation usually does ($2 \leq$ polydispersity index ≤ 3).[32] At 950 rpm, the variation in the zirconocene structure did not influence the polydispersity indices of the resulting copolymers. By contrast, in homopolymerization, Ind_2ZrCl_2, unlike $Et(Ind)_2ZrCl_2$, resisted the broadening of the molecular weight distribution (polydispersity index $\approx$ 2.4, Table II). The reason is that Ind_2ZrCl_2 was stabler than was $Et(Ind)_2ZrCl_2$ during the course of polymerization (see curves H1 and H2 of Fig. 3). The reverse was the effect of the structural variation of the zirconocenes on the copolymer polydispersity index obtained at 450 rpm. Broadening the polydispersity index means the presence of substantially high molecular weight components, which will effectively prevent intimate mixing with additive masterbatches and other polymers on a molecular

level. This will eventually cause processing problems.

Figure 4 compares the differential molecular weight distributions of the experimental polymers. For both the zirconocenes, the peak molecular weights and the molecular weight distributions of the resulting copolymers did not significantly vary with increase of the impeller speed from 450 to 950. This occurred despite variation of the reaction exotherm profiles, that is, the polymerization history from one run to other (see Fig. 3). However, the peak molecular weight fractions, in each case, slightly dropped with increase in the impeller speed. $Et(Ind)_2ZrCl_2$ produced more higher-weight copolymer backbones than did Ind_2ZrCl_2. In homopolymerization, the effect of the zirconocene structural variation on the polymer backbones was reversed, that is, Ind_2ZrCl_2 produced more higher-weight polymer backbones than did $Et(Ind)_2ZrCl_2$. The overall variation in the polydispersity indices (see Table II) and the molecular weight distributions (see Fig. 4) may be attributed to the varying degrees of the chain-termination rate due to β-H elimination, chain transfer by hexene-1, and the σ-bond metathesis reaction.

The side-chain branching in the copolymer backbone, resulting from hexene-1 incorporation, varied more with the variation of the zirconocene structure than with the impeller speed. $Et(Ind)_2ZrCl_2$ incorporated more butyl side chains than did Ind_2ZrCl_2. Consequently, the $Et(Ind)_2ZrCl_2$-based copolymers had a higher hexene-1 content and less crystallinity and density (see Tables I and II) than did the Ind_2ZrCl_2-based ones. Uozumi and Soga[35] observed the same in the isothermal copolymerization of ethylene and hexene-1 catalyzed by $Et(H_4Ind)_2ZrCl_2$ and Cp_2ZrCl_2 in the presence of the MAO cocatalyst; $Et(H_4Ind)_2ZrCl_2$ incorporated more hexene-1 than did Cp_2ZrCl_2. Also, $Et(Ind)_2ZrCl_2$ incorporated more propylene than did Ind_2ZrCl_2 in the copolymerization of ethylene with propylene.[28,31]

All the above studies, including the current one, show that a $C_{2\nu}$ symmetric, chiral (bridged) structure incorporates the comonomer more than did the $C_{2\nu}$ symmetric, achiral (unbridged) one. This can be explained as follows: In each of these published studies, the calculated reactivity ratios show that for the bridged zirconocene the reactivity of ethylene toward the comonomer and vice versa exceeded those of ethylene and the comonomer toward themselves. This means that constraining the rear edge of Ind_2ZrCl_2 with the Et bridge widened the catalytic site for the incorporation of the hexene-1 comonomer in the copolymer backbone.

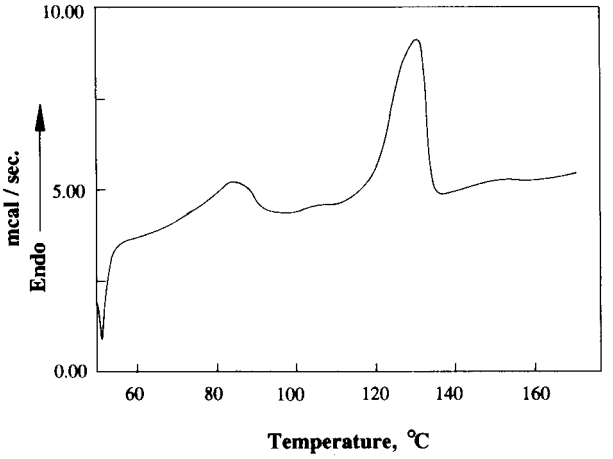

Figure 5 DSC thermogram of the copolymer sample resulting from Run C3.

The above effect of the constrained geometry due to the Et bridge was also reflected in the resulting soluble fractions. $Et(Ind)_2ZrCl_2$ produced more soluble fractions (mainly highly branched materials) at 450 rpm (13.7%) than at 950 rpm (6.6%), whereas for Ind_2ZrCl_2, the opposite was the finding. This explains the importance of optimizing the mixing condition with respect to the polymer properties. The current soluble fraction values are higher than that ($\sim$ 1%) reported for an isothermal metallocene-catalyzed ethylene–octene-1 copolymer.[36] The production of the above high soluble fraction is also evident in the corresponding DSC thermogram (see Fig. 5). The segregated, bimodal DSC thermogram implies that the resulting copolymer will melt at varying temperatures, causing processing inhomogeneity.

Figure 6 shows how the zirconocene structure and the mixing level influenced the copolymer composition distribution measured qualitatively by the CRYSTAF technique. Under the experimental polymerization conditions, increasing the impleller speed from 450 to 950 rpm did not significantly change the composition distributions generated by the unbridged Ind_2ZrCl_2. The composition distributions (see curves C1 and C2 of Fig. 6) remained almost as broad as before despite variation of the interrun reaction exotherm profiles (see curves C1 and C2 of Fig. 3). However, each of these exotherm profiles remained fairly steady, which explains why the corresponding composition distributions did not significantly change.

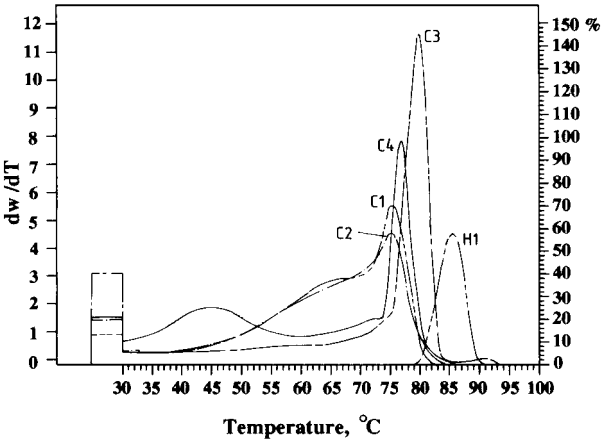

Figure 6 Effect of zirconocene structures and impeller speed on copolymer composition distributions. C1: 450 rpm, Ind_2ZrCl_2; C2: 950 rpm, Ind_2ZrCl_2; C3: 450 rpm, $Et(Ind)_2ZrCl_2$; and C4: 950 rpm, $Et(Ind)_2ZrCl_2$. H1 (950 rpm, Ind_2ZrCl_2) is plotted as a reference.

With the bridged $Et(Ind)_2ZrCl_2$, on the contrary, an increase in the impeller speed converted a long-tailed, monomodal composition distribution into a segregated, multimodal one (compare curve C3 with curve C4 in Fig. 6). Consequently, the performance and application of the Ind_2ZrCl_2-based copolymers will differ from those of the $Et(Ind)_2ZrCl_2$-based ones. Better end uses, especially food packaging, require a minimum level of a soluble fraction in the synthesized copolymers. Note that the average copolymer composition, expressed in terms of chain branching and average hexene-1 content (see Table II), does not reflect these microstructural composition changes.

The above multimodality physically represents preferential incorporation of hexene-1 into the main polymer chain. A comparison of the composition distributions generated by Ind_2ZrCl_2 and $Et(Ind)_2ZrCl_2$ also reflects that the former produced less chain branching than did the latter. The density and average chain branching values (see Tables I and II) support this finding.

CONCLUSIONS

Based on the results of the current study, we conclude the following:

- Nonisothermal, uncontrolled polymerization conducted in varying mixing regimes can illustrate the influence of a number of important process development factors such as mixing, reaction exotherm, kinetic stability of the experimental metallocenes, and thermal perturbations on the catalytic activity, polymerization performance, and the properties of the resulting polymers.
- The reaction exotherm profiles, resulting from the metallocene-catalyzed ethylene homo- and copolymerization, traced the polymerization history. On a qualitative basis, they represented the kinetic profile and the catalytic stability. The unbridged Ind_2ZrCl_2 was shown to be kinetically more stable than the bridged $Et(Ind)_2ZrCl_2$.
- With the change in the level of stirring from a diffusion-controlled regime to a nondiffusion-controlled, external gas–liquid mass-transfer resistance-free one, the following occurred: More thermal perturbation was introduced; the reaction exotherm and the run-time-averagd catalytic activity increased. $Et(Ind)_2ZrCl_2$ produced a segregated, multimodal copolymer composition distribution, illustrating preferential incorporation of hexene-1 into the main polymer chain, whereas Ind_2ZrCl_2 did not significantly influence the same. $Et(Ind)_2ZrCl_2$ produced more soluble fractions; however, the opposite was the finding with Ind_2ZrCl_2. The peak copolymer molecular weights and the molecular weight distributions were not significantly altered but the peak molecular weight fractions dropped.
- Unlike the copolymer composition distribution and soluble fraction, diffusion-controlled and nondiffusion-controlled, external gas–liquid mass-transfer resistance-free regimes of mixing did not significantly affect, the bulk polymer properties such as density, percent crystallinity, average chain branching, and average copolymer composition.
- The peak melting temperatures and the weight- and number-average solution crystallization temperatures (T_w and T_n, respectively) of the copolymers were higher than those of the homopolymers. The reverse was observed with the ratio of $T_w : T_n$.
- The structural variation (bridged versus unbridged) of the zirconocenes so affected the polymerization that at 950 rpm Ind_2ZrCl_2 and $Et(Ind)_2ZrCl_2$ showed a comparable copolymerization catalyst activity; however, at 450 rpm, the reverse was observed. $Et(Ind)_2ZrCl_2$ produced higher molecular

weight backbones, incorporated more hexene-1 and chain branching, and introduced less crystallinity in the resulting copolymers than did Ind_2ZrCl_2. The influence of Ind_2ZrCl_2 on higher-weight homopolymer backbones was the opposite of that of $Et(Ind)_2ZrCl_2$.

- The polydispersity indices expanded with increase in the thermal perturbations.
- Incorporation of hexene-1 significantly decreased the average molecular weights and density and increased the run-time-dependent average catalyst activity. A positive comonomer effect occurred.

The authors acknowledge the support provided by the Research Institute of the King Fahd University of Petroleum & Minerals at Dhahran, Saudi Arabia, for the present study. They also gratefully thank Dr. Benjamin Monrabal of PolyChar of Spain for the CRYSTAF analysis. The molecular weight characterization done by Polymer Laboratories, UK, using GPC 210, and the donation of hexene-1 by Chevron, Switzerland, are highly appreciated.

REFERENCES

1. E. Giannetti, G. M. Nicoletti, and R. Mazzocchi, *J. Polym. Sci. Part A Polym. Chem.,* **23,** 2117 (1985).
2. J. C. W. Chien and B. P. Wang, *J. Polym. Sci. Part A Polym. Chem.,* **26,** 3089 (1988).
3. W. Kaminsky and R. Steiger, *Polyhedron,* **7,** 2375 (1988).
4. J. C. W. Chien and A. Razavi, *J. Polym. Sci. Part A Polym. Chem.,* **26,** 2369 (1988).
5. K. Heiland and W. Kaminsky, *Makromol. Chem.,* **193,** 601 (1992).
6. G. F. Schmidt and W. M. Coleman, in *Transition Metal Catalyzed Polymerizations: Ziegler-Natta and Metathesis Polymerization,* R. P. Quirk and R. E. Hoff, Eds., Cambridge University Press, Cambridge, U.K., 1988, p. 151.
7. M. Atiqullah and E. B. Nauman, *Chem. Eng. Sci.,* **45,** 1267 (1990).
8. M. Atiqullah, M. M. Hassan, and S. A. Beg, *J. Appl. Polym. Sci.,* **46,** 879 (1992).
9. M. Atiqullah, *Eur. Polym. J.,* **29,** 1581 (1993).
10. L. L. Böhm, *Polymer,* **19,** 553 (1978).
11. G. Tosun, *AIChE. J.,* **38,** 425 (1992).
12. The Research Institute, *An Overview of Recent Technological Developments in the Manufacturing of Linear Low and High Density Polyethylenes,* King Fahd University of Petroleum and Minerals, Dhahran, Saudi Arabia, 1991, pp. 5–29.
13. M. Atiqullah, A. K. M. S. Rahman, and S. M. J. Zaidi, *Polym. Eng. Sci.,* **33,** 1644 (1993).
14. H. W. Turner, Eur. Pat. 0,226,463 (June 1987).
15. H. W. Turner, Int. Pat. WO 87/03,604 (Dec. 1987).
16. A. Winter, V. Dolle, M. Antberg, J. Rohrmann, and W. Spleck, Austral. Pat. AU-A-39,056/89 (1990).
17. W. Spaleck, A. Martin, B. Ludwig, R. Jurgen, and L. Hartmut, Can. Pat. 2,017,190 (Nov. 1990).
18. J. A. M. Canich, Int. Pat. WO 91/04,257 (April 1991).
19. J. A. M. Canich, Eur. Pat. 0,420,436 A1 (April 1991).
20. I. Kim, J. H. Kim, and S. I. Woo, *J. Appl. Polym. Sci.,* **39,** 837 (1990).
21. I. Kim, H. K. Choi, J. H. Kim, and S. I. Woo, *J. Appl. Polym. Sci.,* **52,** 1739 (1994).
22. B. Wunderlich and C. M. Cromier, *J. Polym. Sci. Part A 2,* **5,** 987 (1967).
23. B. Monrabal, *J. Appl. Polym. Sci.,* **52,** 491 (1994).
24. B. Monrabal, presentation note, *Polymer ChAR,* Spain, 1996.
25. ASTM D2238 (1986), p. 227.
26. ASTM D1505 (1985), p. 466.
27. L. I. Kulin, N. L. Meijerink, and P. Stock, *Pure Appl. Chem.,* **60,** 1404 (1988).
28. J. C. W. Chien and D. He, *J. Polym. Sci. Part A Polym. Chem.,* **29,** 1585 (1991).
29. J. Koivumäki and J. V. Seppälä, *Macromolecules,* **26,** 5535 (1993).
30. J. C. W. Chien and T. Nozaki, *J. Polym. Sci. Part A Chem.,* **31,** 227 (1993).
31. C. Lehtinen and B. Löfgren, *Eur. Polym. J.,* **33,** 115 (1997).
32. The Research Institute, *Development of Heterogeneous Metallocene Catalysts for Olefin Polymerization. Phase I: Comprehensive Literature Review,* King Fahd University of Petroleum and Minerals, Dhahran, Saudi Arabia, 1996, 295 pp.
33. I. Lee, W. J. Gauthier, J. M. Ball, B. Iyengar, and S. Collins, *Organometallics,* **11,** 2115 (1992).
34. J. Seppälä, *J. Appl. Polym. Sci.,* **30,** 3545 (1985).
35. T. Uozumi and K. Soga, *Makromol. Chem.,* **193,** 823 (1992).
36. B. Monrabal, *Private communication* (Feb. 1997) .